Climatic Change
https://doi.org/10.1007/s10584-020-02841-z

Projected precipitation changes over China for global warming levels at 1.5 °C and 2 °C in an ensemble of regional climate simulations: impact of bias correction methods

Lianyi Guo[1,2] · Zhihong Jiang[1] · Deliang Chen[2] · Hervé Le Treut[3] · Laurent Li[3]

Received: 17 August 2019 / Accepted: 19 August 2020/Published online: 27 August 2020

Abstract

Four bias correction methods, i.e., gamma cumulative distribution function (GamCDF), quantile–quantile adjustment (QQadj), equidistant cumulative probability distribution function (CDF) matching (EDCDF), and transform CDF (CDF-t), to read are applied to five daily precipitation datasets over China produced by LMDZ4-regional that was nested into five global climate models (GCMs), BCC-CSM1-1m, CNRM-CM5, FGOALS-g2, IPSL-CM5A-MR, and MPI-ESM-MR, respectively. A unified mathematical framework can be used to define the four bias correction methods, which helps understanding their natures and essences for identifying the most reliable probability distributions of projected climate. CDF-t is shown to be the best bias correction method based on a comprehensive evaluation of different precipitation indices. Future precipitation projections corresponding to the global warming levels of 1.5 °C and 2 °C under RCP8.5 were obtained using the bias correction methods. The multi-method and multi-model ensemble characteristics allow to explore the spreading of projections, considered a surrogate of climate projection uncertainty, and to attribute such uncertainties to different sources. It was found that the spread among bias correction methods is smaller than that among dynamical downscaling simulations. The four bias correction methods, with CDF-t at the top, all reduce the spread among the downscaled results. Future projection using CDF-t is thus considered having higher credibility.

Keywords Climate downscaling · Bias correction · Daily precipitation · 1.5 °C and 2 °C global warming · Climate projection uncertainty

Electronic supplementary material The online version of this article (https://doi.org/10.1007/s10584-020-02841-z) contains supplementary material, which is available to authorized users.

✉ Zhihong Jiang
zhjiang@nuist.edu.cn

Extended author information available on the last page of the article

1 Introduction

To simulate future climate change scenarios, global climate models (GCMs) are indispensable tools. GCMs are generally reliable in simulating large-scale climate, but are not able to accurately describe regional climate, due to their coarse spatial resolution. Regional climate models (RCMs) are thus necessary in order to dynamically downscale outputs of GCMs. Actually, a number of RCMs including LMDZ, PRECIS, WRF, and RegCM4 have been used in China with demonstrated value added and ability in realistically simulating seasonal variations and spatial distribution of the regional precipitation (Yu et al. 2015; Yang et al. 2016; Zhang et al. 2017).

RCMs have biases in their simulated regional climate, which can be caused by deficiencies in RCMs themselves (such as imperfect parameterizations) and/or by biases from driving GCMs which provide initial and boundary conditions for RCMs (Dosio and Paruolo 2011). In many cases, such biases are not small enough for outputs of RCMs to be directly used for assessment of climate change impacts at a regional scale. It is therefore necessary to find and apply appropriate ways to remove or reduce the biases.

Bias correction is a widely used practice in the current literature (Seneviratne and Nicholls 2012) with some variants in its technical realization. Among them, the quantile mapping method (QM) is based on a simple idea of adjusting the cumulative probability distribution function (CDF) of the simulated variables to match that of observation. The major advantage of this method is that it adjusts all moments (i.e., the entire distribution matches that of the observations for the control period) while maintaining the rank correlation between models and observations. However, it ignores potential changes in the CDF of meteorological variables under the background of future climate change (Panofsky et al. 1958; Wood et al. 2004; Sharma et al. 2007), which can be problematic.

To remediate this issue, Michelangeli et al. (2009) proposed the transform cumulative distribution function (CDF-t) method with the idea of constructing a transfer function (TF) between the observation and simulation during the calibration period. It was shown that CDF-t generally behaves in a much better way than QM does, especially for simulating extreme values (Michelangeli et al. 2009; Sun et al. 2011; Vrac et al. 2012).

Li et al. (2010) proposed a bias correction method which introduces a shift of the CDFs and allows the consideration of changing probability distribution function (PDF) under climate change. Under the title of the equidistant cumulative distribution function matching (EDCDF) method, the methodology consists of translating the difference between the observed CDF and the modeled one during the control period into the CDF of future climate for all given percentiles.

In parallel, Amengual et al. (2012) proposed a quantile–quantile adjustment method (QQadj) with the idea of adjusting quantiles and variances of simulated daily precipitation series. They used a nonparametric function to correct mean, variance, and shape errors of the CDF. They applied QQadj to correct multi-model dynamical downscaling simulations over a small Spanish Mediterranean costal area and showed that QQadj results in clear improvements in mean, variabilities, and probability distribution of the studied variables. However, QQadj applied on bounded variables could produce anomalous behaviors in some situations. Specially, projected quantiles should always remain nonnegative, but admittedly, this requirement cannot be generally guaranteed. For example, negative winds or negative rainfalls do not make any physical sense and must be avoided.

For all these bias correction methods, many interesting results were reported in the literature for different regions and with varied performances (Lavaysse et al. 2012; Lafon et al. 2013;

Tramblay et al. 2013; Yang et al. 2017; Guo et al. 2018). Simultaneously, the European Union founded the VALUE project, which provides an active research network devoted to validation and development of climate downscaling in Europe (Maraun et al. 2015). There is, however, a lack of systematic comparison of different downscaling schemes and approaches for their performances in reproducing climate in East Asia. A recently available ensemble of climate change downscaling simulations for China provides us the opportunity to do just that. We would like to take precipitation simulations to perform such a comparison and to provide reliable future projections based on a number of evaluated bias correction methods. China is located in the East Asian monsoon region with complex terrain. Diverse climatic conditions and frequent extreme climate events can occur in the region and provide an interesting test bed for methods of bias correction.

The study presented here is in the general framework of climate change assessment under two different global warming levels of 1.5 °C and 2 °C above the pre-industrial targets recommended by the 2015 Paris Agreement (UNFCC 2015). The special report on impacts of global warming of 1.5 °C recently issued by the Intergovernmental Panel on Climate Change (IPCC) shows that compared with the 2 °C global warming target, the 1.5 °C target may drastically reduce the frequency and intensity of extreme events (Schaeffer et al. 2012; Knutti et al. 2016). Projected changes of precipitation in China under 1.5 °C and 2 °C targets have been reported in recent literature. Yang et al. (2018) used a statistically downscaled and bias-corrected dataset as performed by Wood et al. (2004) from outputs of the CESM (Community Earth System Model) low-warming experiment. However, Zhai et al. (2017), Li et al. (2018), and Wang et al. (2018) used direct outputs of GCMs from the Coupled Model Intercomparison Project Phase 5 (CMIP5) for future precipitation changes over China. There is generally a large disagreement in the future projections of precipitation in China using different climate models and downscaling methods.

This study intends to revisit the issue of precipitation changes, with an independent dataset that was produced with a regionally oriented climate model forced by multiple GCMs. To increase the reliability, we also perform bias correction to the dynamically downscaled simulations. The four bias correction methods presented above are used and compared with each other, to find out the most reliable method for future precipitation projections over China.

The outline of this paper is as follows. Section 2 describes data and methodology. Section 3 presents a comparison of the four bias correction methods applied to daily precipitation from the RCM. Section 4 provides future changes in mean and extreme precipitation over China under the global warming of 1.5 °C and 2 °C. Furthermore, we also explore and compare the differences among different methods and models. Finally, Section 5 gives a general discussion and conclusion.

2 Data and methodology

2.1 Datasets

The RCM used is LMDZ4 (Hourdin et al. 2006). It is zoomed in East Asia with zoom center at 30° N and 110° E and a domain covering 5~55° N and 85~135° E. The spatial resolution of the model is approximately 0.6° × 0.6°. The key physical processes used in the model correspond to the atmospheric component of the IPSL-CM5A couple model, as described in Li (1999), Hourdin et al. (2006), and Dufresne et al. (2013). Five GCMs from the CMIP5 archive were

used as drivers for LMDZ4, including BCC-CSM1-1-m, CNRM-CM5, FGOALS-g2, IPSL-CM5A-MR, and MPI-ESM-MR, as shown in Table S1. LMDZ4 is used in its regional configuration, and its main variables are nudged by 6 hourly outputs of the GCMs. The nudged variables include zonal wind, meridional wind, temperature, and specific humidity. The downscaling method is a one-way nesting approach, which means that there is no feedback from RCM to GCMs. Our bias correction procedure is divided into three periods: calibration period (1961–1980), validation period (1986–2005), and projection period (2006–2100).

It is to be noted that Yang et al. (2016) evaluated some spatial and temporal patterns of the downscaled climate of China with LMDZ4 when it was nested into three GCMs: BCC-csm1-1-m, FGOALS-g2, and IPSL-CM5A-MR. Their assessment included trends during the last 40 years, statistical properties of sub-regions, and seasonal cycle of rainfall and surface air temperature. LMDZ4 did show its superiority, compared with GCMs, which is due to its more realistic representation of regional terrain including the Tibetan Plateau, the Sichuan Basin, and the Qilian Mountains. In the present work, two other GCMs (CNRM-CM5 and MPI-ESM-MR) are used to extend the ensemble size from three to five.

The 0.5° × 0.5° daily precipitation dataset (Chen et al. 2010), deduced from 753 stations of the China Meteorological Administration network, is used as an observational reference. For the convenience of comparison, we used a bilinear interpolation to convert daily precipitation of LMDZ4 into the grid of 0.5° × 0.5°. More detailed information is shown in Table S1. Our study area covers Central and Eastern China (19.75–53.75° N, 86.25–134.25 °E) with a part of Western China excluded, due to a configuration limitation of LMDZ4.

2.2 Bias correction methods

One of the goals of our study is to provide the climate users a more reliable future projection of daily precipitation over China. To meet this objective, we need to remove biases of the daily precipitation generated by multi-model dynamical downscaling. We want to improve simulations of both the number of rainy days and daily precipitation intensity. In view of the significant seasonal and spatial variation of precipitation in China, we perform our bias correction for each grid cell and each month.

Considering the fact that daily precipitation generated by the RCM has many false small values, it is necessary to firstly define a threshold, in such a way that a non-rainy day is declared when the daily precipitation is below this threshold. The introduction of the threshold is important since it directly impacts the precipitation probability distribution which is the starting point for all CDF-based bias correction methods. One straightforward solution would be to choose an appropriate threshold which makes the simulated daily precipitation sequence of the calibration period possess the same number of non-rainy days as in the observation. But, this method may not be appropriate for future climate. In this work, we decided to use an approach proposed by Amengual et al. (2012) to deduce Z_{CF}, the adjusted number of non-rainy days for the future period:

$$Z_{CF} = (Z_{MF}/Z_{MH})Z_{OH} \tag{1}$$

where Z_{OH} is the number of non-rainy days for the observed precipitation sequence during the calibration period, and Z_{MF}/Z_{MH} denotes the ratio of the number of non-rainy days for the simulation during the future and calibration periods. In practice, a threshold of 0.1 mm/day

was firstly used to discriminate the non-rainy days Z_{OH} in observation. It is then applied to both historical and future simulated time series to obtain Z_{MH} and Z_{MF}. The proportional formula (Eq. 1) can now be used to obtain Z_{CF} which constitutes a constraint for us to define the right threshold leading to the expected future Z_{CF}. Four bias correction methods based on QM were applied to daily precipitation generated by multi-model dynamical downscaling. We evaluate the performance of each method by investigating PDF of daily precipitation and spatial distribution of a number of precipitation indices, and then select the best method to investigate the behaviors of future changes in daily precipitation over China under the global warming of 1.5 °C and 2 °C.

In this paper, let F_{OH} and F_{MH} designate the CDF of the observed and modeled daily precipitation during the calibration (or historical) period, respectively; F_{MF} and F_{CF} denote the CDF of the simulated and corrected precipitation during the future (or our target) period. In what follows a brief description of the four bias correction methods is presented.

2.2.1 Gamma cumulative distribution function matching method

We assume that the CDF of daily precipitation for each grid point matches a gamma distribution for both observed and modeled daily precipitation.

$$F(x;\alpha,\beta)=\frac{1}{\beta^{\alpha}\Gamma(\alpha)}x^{\alpha-1}\exp\left(-\frac{x}{\beta}\right);x\geq 0 \tag{2}$$

where α is a shape parameter, β is a scale parameter, x denotes the precipitation amount, and $\Gamma(\alpha)$ represents the gamma function. The basic assumption of gamma cumulative distribution function (GamCDF) is that the CDF of a climatic variable remains unchanged under the background of global warming, even if it may not match the actual situation perfectly (Panofsky et al. 1958; Haddad et al. 1997). It means that the CDF of daily precipitation during the future period is identical to that during the calibration period in our study. We thus obtain:

$$F_{MF}=F_{MH} \tag{3}$$

$$F_{CF}=F_{OH} \tag{4}$$

Substituting Eq. (3) and Eq. (4) into the mapped formula yields an apparent form.

$$X_{CF}=F_{CF}^{-1}(F_{MF}(X_{MF}))=F_{OH}^{-1}(F_{MH}(X_{MF})) \tag{5}$$

where X_{MF} represents the simulated values for the future period. It is noted that F_{CF} is just equal to F_{OH} for GamCDF. Obviously, the stationary assumption about GamCDF can be problematic, since most recent studies did suggest that the CDF of future precipitation changes in time (Michelangeli et al. 2009; Amengual et al. 2012).

2.2.2 Transform cumulative distribution function method

The CDF-t method is based on the assumption that a transfer function T exists, which establishes the relationship between the CDFs of the observation and simulation (Michelangeli et al. 2009).

$$T(F_{\mathrm{MH}}(X)) = F_{\mathrm{OH}}(X) \tag{6}$$

We define $u = F_{\mathrm{MH}}(X)$, and thus $X = F_{\mathrm{MH}}^{-1}(u)$ with $u \in [0, 1]$. Substituting X into Eq. (6) yields a transform T:

$$T(u) = F_{\mathrm{OH}}\left(F_{\mathrm{MH}}^{-1}(u)\right) \tag{7}$$

Assuming that the above relationship will keep valid over the future period (see Eq. (8)), the CDF of corrected output $F_{\mathrm{CF}}(X)$ is as follows.

$$T(F_{\mathrm{MF}}(X)) = F_{\mathrm{CF}}(X) \tag{8}$$

$$F_{\mathrm{CF}}(X) = F_{\mathrm{OH}}\left(F_{\mathrm{MH}}^{-1}(F_{\mathrm{MF}}(X))\right) \tag{9}$$

As an example, the CDF-t correction process works as follows once a function T between CDFs of the historical observation F_{OH} and simulation F_{MH} is established. Take a future projection value $X_{\mathrm{MF}} = 30$, then the CDF of future corrected values $F_{\mathrm{CF}}(30) = F_{\mathrm{OH}}\left(F_{\mathrm{MH}}^{-1}(F_{\mathrm{MF}}(30))\right)$ (Eq. 9, see segment ① in Fig. 1a). Finally, the future corrected value is $F_{\mathrm{CF}}^{-1}(F_{\mathrm{MF}}(30))$ (see segment ② in Fig. 1a).

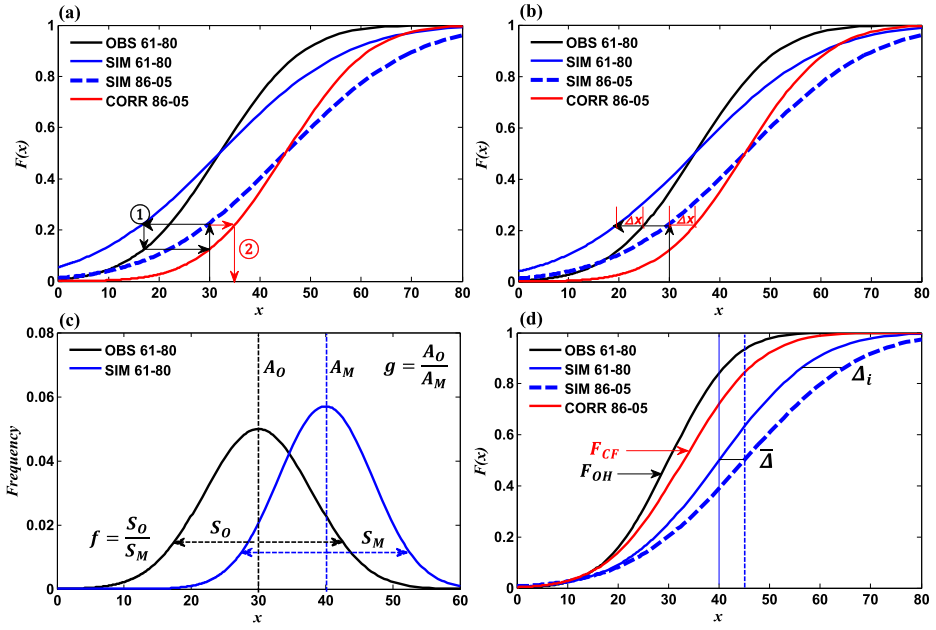

Fig. 1 Schematic illustration of the transform cumulative distribution function method (**a**), equidistant cumulative distribution function matching method (**b**), and quantile–quantile adjustment (**c**, **d**). CDFs of daily precipitation are shown for the observed control (OBS 61-80, black solid curve), raw control (SIM 61-80, blue solid curve), raw validation (SIM 86-05, blue dotted curve), and corrected (CORR 86-05, red solid curve) data. Black (red) arrows denote segment ① (②) for **a**. Δx represents the difference between the observation and the simulation at a specific percentile for **b**. Black and blue dotted vertical lines represent mean values for observations and simulations over the historical period for **c**. Blue solid and dotted vertical lines denote mean values for raw and future simulated period for **d**

2.2.3 Equidistant cumulative distribution function matching method

The method is based on the assumption that for a given percentile, the difference between the modeled and observed values during the calibration period also transmits to the future period, which means that the adjustment function remains the same. However, the difference between the CDFs during the future and historical periods is also considered (Li et al. 2010). The method can be written mathematically as:

$$X_{\mathrm{CF}} = X_{\mathrm{MF}} + {}^{\triangle}x = X_{\mathrm{MF}} + F_{\mathrm{OH}}^{-1}(F_{\mathrm{MF}}(X_{\mathrm{MF}})) - F_{\mathrm{MH}}^{-1}(F_{\mathrm{MF}}(X_{\mathrm{MF}})) \tag{10}$$

where X_{CF} represents the future outputs corrected by using the EDCDF. Figure 1b illustrates the principle of the method after the CDFs were fitted. For the historical observation at each grid, the historical and future simulations follow the Bernoulli–gamma distribution. Take the example of $X_{\mathrm{MF}} = 30$, we can deduce $F_{\mathrm{MF}}(X_{\mathrm{MF}}) = 0.2$. Under the corresponding current climate, the difference between $F_{\mathrm{OH}}^{-1}(0.2)$ and $F_{\mathrm{MH}}^{-1}(0.2)$ is noted as ${}^{\triangle}x$, which can be transposed into the future period. Finally, the corrected value can be deduced as $30 + {}^{\triangle}x$.

2.2.4 Quantile–quantile adjustment

Considering changes in both mean and variance of climate variables under the background of global warming, Amengual et al. (2012) proposed the approach QQadj. It consists of taking the observed CDF, that is F_{OH}, as the corrected F_{CF} for the future, but with adjustments for both mean and variance of the data. The procedure is done at each level i of the percentile with $\Delta_i = F_{\mathrm{MF}}^{-1}(i) - F_{\mathrm{MH}}^{-1}(i)$. Δ_i is the difference between future and historical values for the ith percentile. We can thus obtain the average difference as:

$$\overline{\Delta} = \sum_i \Delta_i \tag{11}$$

which represents the shift of mean values predicted by using the model for the future. Amengual et al. (2012) proposed to adjust this shift following a ratio g of the modeled mean value itself (A_M) to the observed one (A_O):

$$g = A_O / A_M = \sum_i F_{\mathrm{OH}}^{-1}(i) / \sum_i F_{\mathrm{MH}}^{-1}(i) \tag{12}$$

They also proposed to incorporate an additional term to take into account the variance inflation: $f = S_O/S_M$, S_O, and S_M being the standard deviation (SD) of the observed and modeled datasets. Following Amengual et al. (2012), the difference between the 90th and 10th percentiles can be used to approximate SD:

$$S_O = F_{\mathrm{OH}}^{-1}(i_{90}) - F_{\mathrm{OH}}^{-1}(i_{10}) \tag{13}$$

$$S_M = F_{\mathrm{MH}}^{-1}(i_{90}) - F_{\mathrm{MH}}^{-1}(i_{10}) \tag{14}$$

Once the percentile level i is determined by $i = F_{\mathrm{MF}}(X_{\mathrm{MF}})$ for a given X_{MF}, the final variable after the adjustment is:

$$X_{\mathrm{CF}} = F_{\mathrm{CF}}^{-1}(i) = F_{\mathrm{OH}}^{-1}(i) + g\overline{\Delta} + f\left(\Delta_i - \overline{\Delta}\right) \tag{15}$$

Actually, the four methods described above and all other CDF-based correction methods have a similar philosophy but different technical realizations. The basic principle is to deduce a relationship (or a functional) between CDFs of observed and simulated values during the calibration period, or between CDFs of current and future RCM's outputs, and then apply it in the calculation of the CDF of future period simulations. Therefore, constructing the CDF of corrected outputs during the future period F_{CF} is the key element for each method. Once F_{CF} is available, the corrected value X_{CF} can be written mathematically as:

$$X_{CF} = F_{CF}^{-1}(F_{MF}(X_{MF})) \tag{16}$$

where X_{MF} represents the simulated values during the future period.

To sum up, if we want to use a unified mathematical framework to define the four bias correction methods, we can formally write F_{CF} as follows.

$$\begin{cases} F_{CF}(X) = F_{OH}(X) & \text{GamCDF} \\ F_{CF}(X) = F_{OH}\left(F_{MH}^{-1}(F_{MF}(X))\right) & \text{CDF-t} \\ F_{CF}\left(X + F_{OH}^{-1}(F_{MF}(X)) - F_{MH}^{-1}(F_{MF}(X))\right) = F_{MF}(X) & \text{EDCDF} \\ F_{CF}\left(X + g\overline{\Delta} + f\left(\Delta_i - \overline{\Delta}\right)\right) = F_{OH}(X) & \text{QQadj} \end{cases} \tag{17}$$

The first two formulas are quite obvious, but the last two ones need some explanations for their obtention. For the case of EDCDF, we combine Eqs. (10) and (16) to deduce an intermediate equation:

$$X + F_{OH}^{-1}(F_{MF}(X)) - F_{MH}^{-1}(F_{MF}(X)) = F_{CF}^{-1}(F_{MF}(X)) \tag{18}$$

which permits us to obtain the final form as in Eq. (17).

For the case of QQadj, we define $i = F_{OH}(X)$ and deduce $X = F_{OH}^{-1}(i)$ with $i \in [0, 1]$. Since Eq. (15) can be transformed into:

$$X_{CF} = X + g\overline{\Delta} + f\left(\Delta_i - \overline{\Delta}\right) \tag{19}$$

and

$$F_{CF}(X_{CF}) = i \tag{20}$$

we can easily obtain the final form by introducing Eq. (19) and $i = F_{OH}(X)$ into Eq. (20).

2.3 Precipitation indices and evaluation methods

Four indices including total precipitation (PRCPTOT), precipitation intensity (SDII), number of rainy days for daily precipitation more than 10 mm (R10mm), and maximum consecutive dry days (CDD) are used to measure climate characteristics of simulated precipitation, and their definitions are given in Table S2. They are calculated with the diagnostic software provided by the statistical and regional dynamical downscaling of extremes for European regions (Haylock et al. 2006). A parameter assessing the distribution of daily precipitation, skill score S_{score} (Perkins et al. 2007), and another describing the spatial pattern agreement in terms of the Taylor diagram (Taylor 2001) are used to measure the performance of the four bias correction methods.

S_{score} measures the similarity between the observed and modeled PDFs by calculating the cumulative minimum value of two distributions. If a model simulates the observed PDF poorly, S_{score} is close to 0 with negligible overlap between the two PDFs.

The Taylor diagram provides a statistical summary of comparisons between simulations and observations in terms of their spatial correlation coefficient, their centered root-mean-square difference, and the ratio of spatial standard deviations of the model and observations. A perfect simulation would be that the centered root-mean-square error (RMSE) is equal to 0, and both the spatial correlation coefficient and ratio of spatial standard deviations are close to 1.

2.4 Timing determination for the global warming levels of 1.5 °C and 2 °C

Time series of global mean temperature anomalies under the RCP8.5 emission scenario is smoothed by a 21-year moving average, and the 1.5 °C and 2 °C global warming thresholds, which are firstly reached, are selected relative to the pre-industrial period (1861–1900). Finally, the consecutive 10 years before the crossing point, together with the consecutive 10 years after the crossing point, form our investigation period of 21 years. It is noted that changes of climate variables in this study are accounted relative to the current reference period (1986–2005), as generally practiced in this field of research.

For the timing of 1.5 °C and 2 °C global warming levels, there exists an overlap for almost all models as shown in Table S3. King et al. (2017) pointed out that although individual years may contribute to both the 1.5 °C and 2 °C ensembles, none of the analysis assumes independence between the two worlds. They furthermore found that using a narrower range reduced the sample size but made little difference after all. We also remind that many previous studies selected the time window of 21 years (Shi et al. 2018; Yu et al. 2018), and even 31 years (Hu et al. 2017; Wang et al. 2018), with a larger overlap.

3 Evaluation of the four bias correction methods

In this section, we use the four bias correction methods (GamCDF, QQadj, EDCDF, and CDF-t) to improve the daily precipitation simulated by LMDZ4 (zoom version over East China) driven by five GCMs. We put emphasis on the benefits of the bias correction compared with performance of the original RCM simulations. We focus on evaluating the properties in relation to the probability distribution of daily precipitation and the spatial patterns of the selected precipitation indices (PRCPTOT, SDII, R10mm, and CDD) during the validation period (1986–2005).

3.1 Statistical properties of daily precipitation

To evaluate the statistical properties of daily precipitation, we firstly show the quantile–quantile plots deduced from the 20-year daily precipitation time series for six grid points located in the Tibetan Plateau, Southwest China, Northeast China, North China, South China, and middle and low reaches of the Yangtze River, respectively (Fig. 2). Results are displayed in a single array gathering all RCM simulations without referring to any particular one. We did not average the simulations before calculating percentiles in order to preserve the whole probability distribution of precipitation. LMDZ simulations are significantly lower than the

observation within a threshold, but larger than the observed one when exceeding that threshold for each of the selected grid points. This behavior of LMDZ is somehow surprising, since most other models underestimate heavy precipitation in their simulation. Our result is nevertheless consistent with Chen et al. (2011) who also found that LMDZ in its high-resolution regional configuration could overestimate heavy precipitation. In our results shown in Fig. 2, the largest difference is above 60 mm/day. After bias corrections, all methods, namely GamCDF, QQadj, EDCDF, and CDF-t, improve the quality of the daily precipitation. However, GamCDF and EDCDF have similar improvements with a performance inferior to that of QQadj and CDF-t. Except for the grid point in North China (Fig. 2d1, d2), CDF-t outperforms QQadj for all other locations.

The corrected precipitation (more than 30 mm/day) from bias correction, such as CDF-t and QQadj, is even worse than the simulated precipitation from the raw RCM outputs in Fig. 2d1. Heavy precipitation is a challenging issue for the arsenal of our current climate simulation, GCM, RCM, statistical downscaling, etc. Bias correction algorithms are also quite often challenged in terms of heavy precipitation. That said, we believe that the fact that the

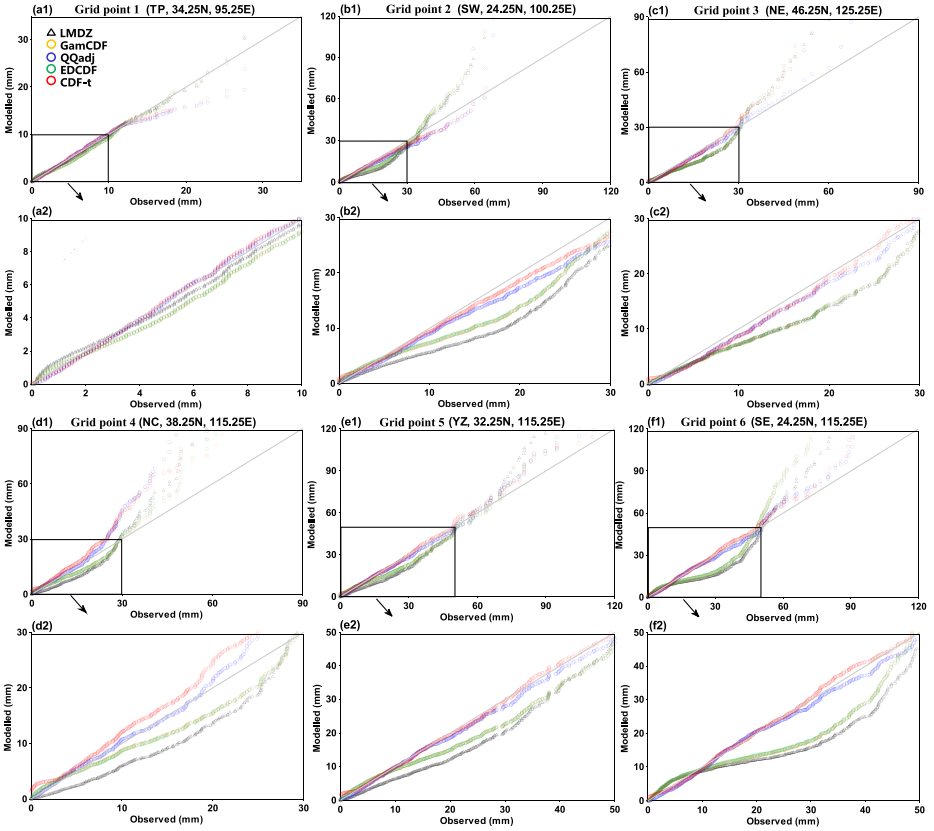

Fig. 2 Quantile–quantile plots of simulated daily precipitation during the validation period (1986–2005) in the multi-model ensemble of RCMs (black), GamCDF (orange), QQadj (blue), EDCDF (green), and CDF-t (red) after correction, and observations at six grid points located in Tibetan Plateau (34.25° N, 95.25° E; a1, a2), southwestern (24.25° N, 100.25° E; b1, b2), northeastern (46.25° N, 125.25° E; c1, c2), northern (38.25° N, 115.25° E; d1, d2), middle and low reaches of the Yangtze River (32.25° N, 115.25° E; e1, e2), and southern region (24.25° N, 115.25° E; f1, f2), respectively

validation period may present significant variation (internal random variability or low-frequency natural variability) from the calibration period can be responsible for some of the performance degradation of our bias correction algorithms. We should anyway recognize that further investigation is needed to achieve a better understanding for this issue.

To evaluate all grid points in the study region, we use the box-and-whisker plot showing the distribution of all S_{score} values which are a measure of the overlapping degree between the two PDFs (Fig. 3). Results indicate that all GamCDF, QQadj, EDCDF, and CDF-t significantly improve the probability distribution of daily precipitation, the medians of S_{score} being 0.95 in LMDZ and increasing to 0.96 in GamCDF, 0.98 in QQadj, 0.96 in EDCDF, and 0.98 in CDF-t, respectively. QQadj and CDF-t show satisfactory results and a significant improvement. However, there is a large spreading of S_{score} for QQadj among different grid points. CDF-t is thus considered the most robust method that is our first choice to correct daily precipitation in the study region.

3.2 Spatial distribution of the precipitation indices

We further assess behaviors of the four bias correction methods in reproducing the spatial pattern of precipitation indices shown in Fig. 4. The observed and simulated mean annual precipitation indices during the validation period (1986–2005) over all the grid cells in the study region before and after correction results are displayed. For the whole year, there is a relatively mediocre performance for direct outputs of RCM. Specifically, spatial correlation coefficients are smaller than 0.70, RMSEs are larger than 0.8 mm, and normalized SDs are between 0.75 and 1.25. After correction, GamCDF, QQadj, EDCDF, and CDF-t all improve the spatial pattern of precipitation indices. CDF-t shows the best overall performance. Except CDD that shows few changes, other indices including PRCPTOT, SDII, and R10mm show obvious improvements with spatial correlation coefficients being increased to higher than 0.88;

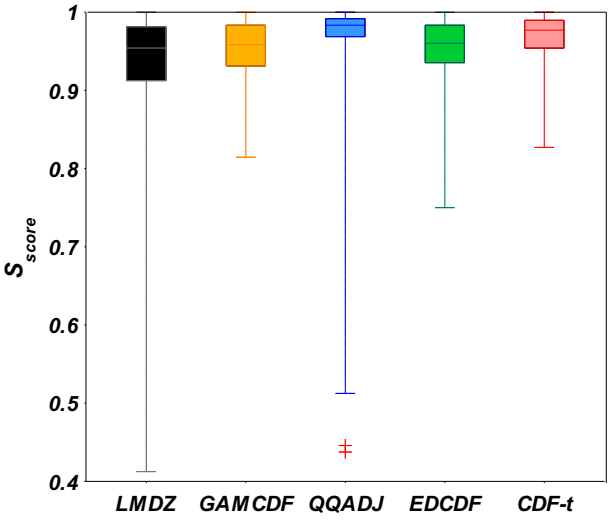

Fig. 3 Box-and-whisker plot (the five-number summary is the minimum, first quartile, median, third quartile, and maximum) of S_{score} measuring PDFs of daily precipitations during the validation period (1986–2005) at all grid points in the study region before (black) and after corrections of GamCDF (orange), QQadj (blue), EDCDF (green), and CDF-t (red)

RMSEs were reduced to less than 0.5; and normalized SDs were kept between 0.90 and 1.10. For the CDF-t method, the spatial correlation coefficient is above 0.95, RMSE is smaller than 0.3, and normalized SD is almost 1.

The fact that only limited (or no) improvements are found for CDD is consistent with the theoretical analysis of Dosio (2016). They also found that indices based on the duration of events are hardly affected by bias adjustment, because bias adjustment does not alter the temporal structure of the original data.

In summary, GamCDF and EDCDF show similar skills in bias-correcting daily precipitation, but inferior performance compared with QQadj and CDF-t. In terms of assumptions underlying the methods, the one behind CDF-t is more physically justified, since it takes into account eventual changes in the CDF from the historical (calibration) to future (projection) times, while GamCDF can only project future values with the historical CDF, which implies that GamCDF cannot provide new values outside historical observations. This can be a clear disadvantage in a changing climate context. CDF-t provides a solution to this problem by taking into account simulated future CDF. As far as EDCDF is concerned, it does consider such change of the CDF for a given percentile, but it assumes an identical shift between the model and observation for both calibration and future projection periods. CDF-t and QQadj both consider CDF changes over time, which is closer to the real world.

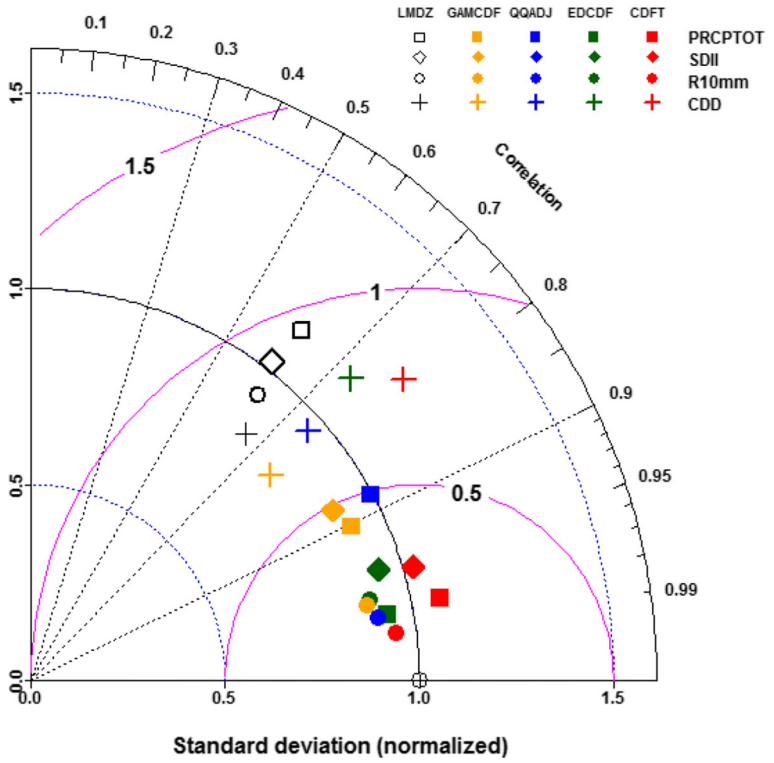

Fig. 4 Taylor diagram showing the performance in reproducing the spatial pattern of four precipitation indices (PRCPTOT, SDII, R10mm, and CDD) during the validation period (1986–2005) before (black) and after corrections using GamCDF (orange), QQadj (blue), EDCDF (green), and CDF-t (red)

Our general approach in conducting this bias correction work can be basically decomposed into three steps: calibration, validation, and application into future climate projection. Our validation is actually the holdout method, which does not totally belong to the category of cross-validation, i.e., we calibrate the method on a calibration period and evaluate it on a non-overlapping validation period. A caveat of this approach is the eventual appearance of misleading results due to strong internal variability of the climate system (Maraun and Widmann 2018). With the necessary precautions in mind, we think that our approach is still a valid and useful one, since the four methods were validated under an identical circumstance.

4 Future projection of precipitation and associated uncertainties

4.1 Changes of mean and extreme precipitation under 1.5 °C and 2 °C warming targets

In this section, we use the bias correction method CDF-t, our best choice as shown in Section 3, to correct future projections simulated by the multi-ensemble regional climate simulations under the global warming of 1.5 °C and 2 °C. Previous studies have shown that regional-scale responses of temperature and precipitation are almost independent of the precise emission scenarios, but are more closely related to the global warming level (Hu et al. 2017; Zhai et al. 2017). Therefore, our future climate analyses are performed only for the RCP8.5 scenario.

The spatial pattern of changes in PRCPTOT, SDII, and R10mm based on CDF-t under the global warming of 1.5 °C and 2 °C, relative to 1986–2005, is shown in Fig. 5. PRCPTOT has an increasing trend in most areas of North China under the global warming of 1.5 °C. The increase is above 60% over Northwest China and 40% over the northern region of Northeast China. A significant increase of PRCPTOT in the northern region of Northeast China is in accord with Wang et al. (2018) using fifteen CMIP5 models without any downscaling or bias correction. However, there is a weak decreasing trend in Central China and south of the Yangtze River, which is consistent with Chen and Sun (2018) using raw outputs from nineteen CMIP5 models. The additional half-degree warming results in an increase in precipitation over Central China and south of the Yangtze River, and a decrease over Northwest China and Northeast China (Fig. 5c).

For SDII, there is an increasing trend over almost whole China under the global warming of 1.5 °C, with a significant increase of over 50% for the southern region of Northeast China (Fig. 5d). The additional half-degree warming from 1.5 to 2 °C implies no obvious difference in spatial characteristics of precipitation with slight decrease in Inner Mongolia and South China (Fig. 5f).

R10mm increases over the northern region of the Yellow River basin, especially in Northeast China, the western region of Northwest China, and the western region of the Tibetan Plateau with a value of above 60% under 1.5 °C warming target, while there are significant decreases over the eastern region of Northwest China and the eastern region of the Tibetan Plateau with a value of more than 40%. Additionally, there is a weak decrease in the south of the Yangtze River in accord with Zhou et al. (2014) using twenty-four CMIP5 models (Fig. 5g). The additional half-degree warming from 1.5 to 2 °C causes a decrease in the north of the Yellow River and an increase in the Yangtze River Basin and in West China (Fig. 5i). The conclusion that SDII and R10mm increase over Northeast China is consistent with Yang et al.

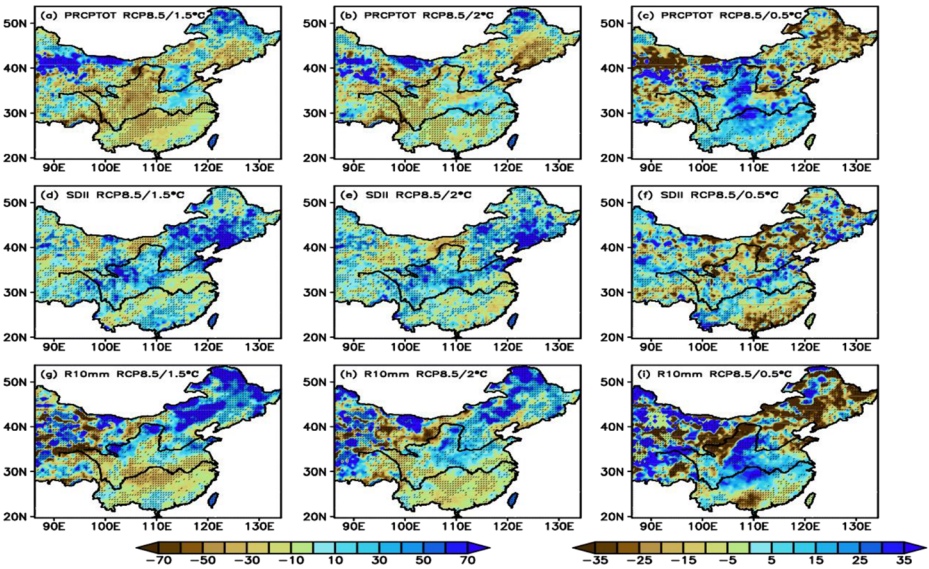

Fig. 5 Relative changes in PRCPTOT (a, b, c), SDII (d, e, f), and R10mm (g, h, i) based on CDF-t under the global warming of 1.5 °C (first column), 2 °C (second column), and the half-degree addition (third column), relative to 1986–2005 (unit: %). The areas which all four methods agree with the sign of change in the raw RCM are indicated by dots

(2018) using a statistical downscaling method from outputs of CESM low-warming experiment.

It is expected that the bias-corrected results are different from the direct outputs of the RCM (Fig. S1, S2, and S3), since the four methods use different strategies to make adjustment on the CDF of the downscaled daily precipitation. However, the spatial patterns of three precipitation indices from the raw RCMs are similar with those from four bias correction methods. Actually, in Fig. 5, the areas marked by dots represent zones where the four methods agree with the sign of change in the raw RCM. Such zones are large and dominant, which proves that the four bias adjustment techniques just remove biases from the outputs of RCM, but largely preserve spatial patterns from RCM simulations.

Following Dosio (2016), we examined the adjustment of the CDF before and after the bias corrections. The difference of frequency between present and future daily precipitation for the original and bias-adjusted RCM is now given in the Supplementary materials (Fig. S4). It displays however only one simulation: LMDZ4 driven by BCC-CSM1-1-m (other simulations show very similar results). It appears that all the four bias correction methods can preserve the statistical properties of the RCM simulation, with nevertheless some subtle differences.

4.2 Uncertainties of the precipitation projection

We now assess issues of uncertainty for precipitation change projection by exploring the multi-method and multi-model characteristics of our approach. Actually, the spreading offered by the collection of available RCM simulations provides a useful proxy to reveal the climate change projection uncertainty. As a climate change scenario provider to policymakers and other end users, we have the responsibility to deal with uncertainty issues when a climate change scenario is released. Our data collection comprises five RCM realizations from five different

GCMs and their bias-corrected data with the four bias correction methods. We examine their spread among the members of the ensemble. Spreading is generally considered an indicator of uncertainties (Knutti and Sedlacek 2013; Chen et al. 2013; Fatichi et al. 2016; Her et al. 2019).

Figure 6 presents the CDFs showing the cumulative probability of relative changes in PRCPTOT, SDII, and R10mm under the global warming of 2 °C. Each curve was constructed with all values over the study region for each of the four bias correction methods and each of the five RCM simulations. The 25 scenarios are grouped by bias correction methods and separated by the RCM simulations, indicating that the uncertainty related to driving GCMs is larger than that linked to bias correction methods, which is consistent with Chen et al. (2013). The CDF curves for PRCPTOT seem to be more dispersed than for SDII and R10mm. It is to be noted that very similar results (not shown) were obtained for projections under the 1.5 °C target.

Beyond the visual inspection which is possible in Fig. 6, we can also use the concept of signal-to-noise ratio (SNR) (as used in Li 1999, and Zhou and Yu 2006) which provides more quantitative measures for uncertainty considerations. In our case of five available dynamic simulations, the SNR can be simply defined as the mean projected changes under 1.5- and 2.0-degree warming targets (signal) divided by the inter-simulation standard deviation (noise). If we calculate the SNR before and after each bias correction method, we can assess how the uncertainty of future climate projection is impacted. Figure 7 provides a boxplot showing the relative changes of SNR for PRCPTOT, SDII, and R10mm using each of the four bias correction methods (compared with raw RCMs) at the 2-degree warming target. There is a clear increase in terms of SNR for the majority of grid points and for the three climate indices. CDF-t shows a satisfactory performance with increasing SNR. We further give the percentage of grid points in the study region where there is an increase of the SNR achieved by bias correction at the two warming targets (Table 1). It is clear that all the four methods reduce the uncertainty among simulation members and enhance the SNR over 73.4~77.7% of areas in the study region for PRCPTOT and SDII, and about 55.7~58.4% of areas for R10mm. In particular, CDF-t significantly decreases the uncertainty for different precipitation indices and warming targets. Finally, we try to clarify why the SNR is larger for the bias-adjusted results. It is a consequence of the slightly larger signal after corrections for most parameters and the significantly smaller noise (inter-model spread) after corrections (Fig. S5).

In summary, the spread among bias correction methods is relatively small, smaller than the spread among dynamical downscaling simulations. It is important to note that all the four methods enhance SNR in our multi-member ensemble approach. This is especially true for CDF-t. We thus consider that future projection using CDF-t in Section 4.1 is of high credibility.

Finally, a summary of shared and distinctive features of the four bias correction methods from the view of the principle and their impact on future projections is given in Table S4.

5 Summary and conclusions

Bias correction is often a necessary step for regionally oriented climate change projections, after performing regional climate simulations, even with a very high spatial resolution. The reason is a quite pragmatic one: many climate impact studies would not be possible if climate information as input has a too large bias. In this work, we implemented four bias correction methods (GamCDF, QQadj, EDCDF, and CDF-t) and apply them to an ensemble of regional

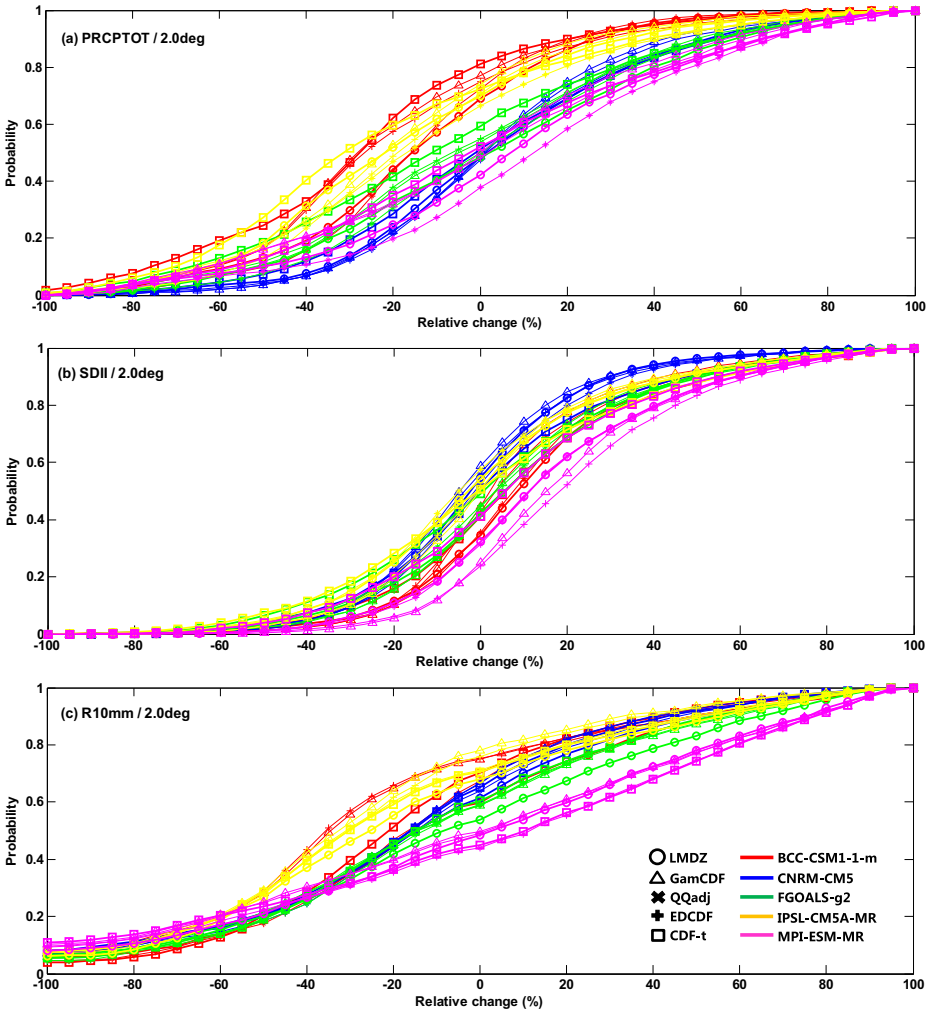

Fig. 6 Cumulative probability distribution functions (CDFs) constructed in the study region for values of relative changes (in %) in PRCPTOT (a), SDII (b), and R10mm (c) under the 2.0-degree warming target. There are 25 curves in the first three panels, with five RCM simulations shown in different colors, and the original (LMDZ) and four bias correction results are shown in different symbols

climate simulations for China performed with LMDZ4-regional that was driven by five global climate models: LMDZ4/BCC-CSM1-1m, LMDZ4/CNRM-CM5, LMDZ4/FGOALS-g2, LMDZ4/IPSL-CM5A-MR, and LMDZ4/MPI-ESM-MR. After a comprehensive evaluation on the probabilistic characteristics (PDF) of daily precipitation and spatial distribution of precipitation indices (PRCPTOT, SDII, R10mm, and CDD), we selected the best-behaved method to further assess future changes of daily precipitation in the study region under the RCP8.5 emission scenario at 1.5 °C and 2 °C targets. Finally, we explored the difference of projections among our different dynamical simulations and bias correction methods to evaluate uncertainties in the projected regional climate changes. Main conclusions can be drawn as follows.

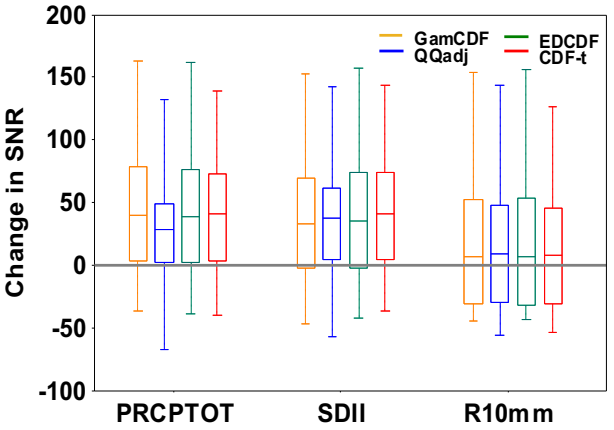

Fig. 7 Boxplot showing relative changes (%) of the signal-to-noise ratio for PRCPTOT, SDII, and R10mm using GamCDF (yellow), QQadj (blue), EDCDF (green), and CDF-t (red) compared with the raw RCMs at 2-degree warming target. The upper and lower limits of the box indicate the 75th and 25th percentiles among all grid points over the study area, the horizontal line inside the box indicates the 50th percentile (median), and the whiskers show the range among all grid points

1) GamCDF, QQadj, EDCDF, and CDF-t can all significantly improve the quality of the RCM simulations in terms of both probability density (PDF) of daily precipitation and spatial patterns of precipitation indices. It was determined that QQadj has the largest improvement and CDF-t is the second one. But the whole range of S_{score} for CDF-t is the smallest among all grid points in the study region, which motivated us to take CDF-t as our privileged bias correction method. Except CDD, other indices such as PRCPTOT, SDII, and R10mm all have significant improvements compared with the raw data from the RCM. For the selected method CDF-t, the spatial correlation coefficient is larger than 0.95, the RMSE is smaller than 0.3, and the SD is almost 1.
2) Under the global warming of 1.5 °C, and after the CDF-t bias correction, PRCPTOT shows an increasing trend in northern China, an increase of more than 60% over Northwest China and more than 40% over the north region of Northeast China. However, there is a weak decreasing trend in Central China and south of the Yangtze River for PRCPTOT. For SDII, there is an increasing trend over almost the whole Chinese territory, with a significant increase by over 50% for the southern region of Northeast China. R10mm increases over the northern region of the Yellow River, Northeast China, the western region of Northwest China, and the western region of the Tibetan Plateau with a value of above 60%.

Table 1 The percentage (%) of grid points in the study region where there is an amelioration of the signal-to-noise ratio achieved by bias correction. The italicized values represent the largest improvement

	1.5 degrees			2.0 degrees		
	PRCPTOT	SDII	R10mm	PRCPTOT	SDII	R10mm
GamCDF	75.8	74.5	57.8	76.0	73.4	55.7
QQadj	76.6	74.1	60.0	75.9	77.6	58.4
EDCDF	78.5	72.4	57.5	75.8	73.4	55.8
CDF-t	*81.2*	*77.3*	*60.0*	*76.3*	*77.7*	*58.4*

3) The spread introduced by using different bias correction methods in the ensemble approach of future climate projection is relatively small and generally smaller than the spread among dynamical downscaling simulations. The four methods all enhance the signal-to-noise ratio by 73.4~77.7% for PRCPTOT and SDII, and by 55.7~58.4% for R10mm. CDF-t shows the best performance in terms of uncertainty reduction for different precipitation indices and warming targets. In our study, actually, the spread among the five simulations is relatively small for their future climate projection in terms of daily precipitation in the study region.

Among the four bias correction methods, GamCDF is a basic and simple method, but its ability of correction is equivalent to EDCDF. CDF-t and QQadj show a more robust behavior and a certain superiority compared with the former two methods. In addition, we found that the performance of each correction method, to a certain extent, also depends on the datasets from the RCM and GCM. The correction plays a more important role if the drift in the RCM is large. Finally, we find that there are disagreements and agreements in future rainfall projections over China between our results and those of other studies. The disagreement mainly results from different GCMs, downscaling and bias correction methods, and transient or equilibrium warming response (Zhou et al. 2014; Zhai et al. 2017; Wang et al. 2018; Chen and Sun 2018; Yang et al. 2018).

Acknowledgments We thank the editor and three anonymous reviewers for their constructive comments.

Funding information This study was supported by the National Key Research and Development Program of China (2017YFA0603804, 2018YFC1507704), the Postgraduate Research and Practice Innovation Program of Government of Jiangsu Province (SJKY19_0930), and the Visiting Fellowship from China Scholarship Council (NO. 201908320544). L. Li acknowledges the support of French ANR (Project China-Trend-Stream). D. Chen is supported by the Swedish STINT and MERGE.

Data availability The interpolated 0.5° × 0.5° daily precipitation datasets are available from the URL (http://rcg.gvc.gu.se/). The LMDZ4 datasets are available from the NEC-SX5 of the IDRIS/CNRS computer center.

References

Amengual A, Homar V, Romero R et al (2012) A statistical adjustment of regional climate model outputs to local scales: application to Platja de Palma, Spain. J Clim 25(3):939–957. https://doi.org/10.1175/JCLI-D-10-05024.1

Chen HP, Sun JQ (2018) Projected changes in climate extremes in China in a 1.5°C warmer world. International Journal of Climatology. https://doi.org/10.1002/joc.5521

Chen D, Ou T, Gong L et al (2010) Spatial interpolation of daily precipitation in China: 1951-2005. Adv Atmos Sci 27(6):1221–1232. https://doi.org/10.1007/s00376-010-9151-y

Chen WL, Jiang ZH, Li L, Yiou P (2011) Simulation of regional climate change under the IPCC A2 scenario in Southeast China. Clim Dyn 36:491–507. https://doi.org/10.1007/s00382-010-0910-3

Chen J, Brissette FP, Chaumont D, Braun M (2013) Performance and uncertainty evaluation of empirical downscaling methods in quantifying the climate change impacts on hydrology over two North American river basins. J Hydrol. https://doi.org/10.1016/j.jhydrol.2012.11.062

Dosio A (2016) Projections of climate change indices of temperature and precipitation from an ensemble of bias-adjusted high-resolution EURO-CORDEX regional climate models. Journal of Geophysical Research: Atmospheres 121:5488–5511. https://doi.org/10.1002/2015JD024411

Dosio A, Paruolo P (2011) Bias correction of the ENSEMBLES high-resolution climate change projections for use by impact models: evaluation on the present climate. J Geophys Res 116(117):127–135. https://doi.org/10.1029/2011JD015934

Dufresne JL, Foujols MA, Denvil S et al (2013) Climate change projections using the IPSL-CM5 Earth System Model: from CMIP3 to CMIP5. Clim Dyn 40(9–10):2123–2165. https://doi.org/10.1007/s00382-012-1636-1

Fatichi S, Ivanov VY, Paschalis A, Peleg N et al (2016) Uncertainty partition challenges the predictability of vital details of climate change. Earth's Future 4:240–251. https://doi.org/10.1002/2015EF000336

Guo LY, Gao Q, Jiang ZH, Li L (2018) Bias correction and projection of surface air temperature in LMDZ multiple simulation over central and eastern China. Adv Clim Chang Res 9(1):81–92. https://doi.org/10.1016/j.accre.2018.02.003

Haddad ZS, Rosenfeld D (1997) Optimality of empirical Z-R relations.Q J R Meteorol Soc 123(541):1283–1293. https://doi.org/10.1002/qj.49712354107

Haylock MR, Cawley GC, Harpham C, Wilby RL, Goodess CM (2006) Downscaling heavy precipitation over the United Kingdom: a comparison of dynamical and statistical methods and their future scenarios. Int J Climatol 26(10):1397–1415. https://doi.org/10.1002/joc.1318

Her Y, Yoo SH, Cho J et al (2019) Uncertainty in hydrological analysis of climate change: multi-parameter vs. multi-GCM ensemble predictions. Scientific Reports 9:4974. https://doi.org/10.1038/s41598-019-41334-7

Hourdin F, Musat I, Bony S et al (2006) The LMDZ4 general circulation model: climate performance and sensitivity to parametrized physics with emphasis on tropical convection. Clim Dyn 27(7–8):787–813. https://doi.org/10.1007/s00382-006-0158-0

Hu T, Sun Y, Zhang XB (2017) Temperature and precipitation projection at 1.5°C and 2°C increase in global mean temperature. Chinses Science Bulletin. https://doi.org/10.1360/N972016-01234

King AD, Karoly DJ, Henley BJ (2017) Australian climate extremes at 1.5 °C and 2 °C of global warming. Nat Clim Chang 7:412–416. https://doi.org/10.1038/nclimate3296

Knutti R, Sedlacek J (2013) Robustness and uncertainties in the new CMIP5 climate model projections. Nat Clim Chang 3:369–373. https://doi.org/10.1038/nclimate1716

Knutti R, Rogelj J, Sedlacek J, Fischer EM (2016) A scientific critique of the two-degree climate change target. Nat Geosci 9(1):13–18. https://doi.org/10.1038/NGEO2595

Lafon T, Dadson S, Buys G, Prudhomme C (2013) Bias correction of daily precipitation simulated by a regional climate model: a comparison of methods. Int J Climatol 33:1367–1381. https://doi.org/10.1002/joc.3518

Lavaysse C, Vrac M, Drobinski P, Lengaigne M, Vischel T (2012) Statistical downscaling of the French Mediterranean climate: assessment for present and projection in an anthropogenic scenario, Natural Hazards and Earth System. Sciences 12:651–670. https://doi.org/10.5194/nhess-12-651-2012

Li ZX (1999) Ensemble atmospheric GCM simulation of climate interannual variability from 1979 to 1994. J Clim 12:986–1001. https://doi.org/10.1175/1520-0442(1999)012<0986:EAGSOC>2.0.CO;2

Li H, Sheffield J, Wood EF (2010) Bias correction of monthly precipitation and temperature fields from Intergovernmental Panel on Climate Change AR4 models using equidistant quantile matching. Journal of Geophysical Research Atmospheres 115(D10). https://doi.org/10.1029/2009JD012882

Li W, Jiang ZH, Zhang XB, Li L, Sun Y (2018) Additional risk in extreme precipitation in China from 1.5°C to 2.0°C global warming levels. Science Bulletin 63(4). https://doi.org/10.1016/j.scib.2017.12.021

Maraun D, Widmann M (2018) Cross-validation of bias-corrected climate simulations is misleading. Hydrol Earth Syst Sci 22:4867–4873. https://doi.org/10.5194/hess-22-4867-2018

Maraun D, Widmann M, Gutiérrez José M et al (2015) VALUE: A framework to validate downscaling approaches for climate change studies. Earths Future 3(1):1–14. https://doi.org/10.1002/2014EF000259

Michelangeli PA, Vrac M, Loukos H (2009) Probabilistic downscaling approaches: application to wind cumulative distribution functions. Geophys Res Lett 36:L11708. https://doi.org/10.1029/2009GL038401

Panofsky HA, Brier GW, Best WH (1958) Some application of statistics to meteorology. Penn State University Tech. Rep. 24pp

Perkins SE, Pitman AJ, Holbrook NJ, Mcaneney J (2007) Evaluation of the AR4 climate models' simulated daily maximum temperature, minimum temperature, and precipitation over Australia using probability density functions. J Clim 20:4356–4376. https://doi.org/10.1175/JCLI4253.1

Schaeffer M, Hare W, Rahmstorf S, Vermeer M (2012) Long-term sea-level rise implied by 1.5°C and 2°C warming levels. Nat Clim Chang 2:867–870. https://doi.org/10.1038/nclimate1584

Seneviratne SI, Nicholls N (2012) Changes in climate extremes and their impacts on the natural physical environment. In Managing the risks of extreme events and disasters to advance climate change adaptation: a special report of working groups I and II of the Intergovernmental Panel on Climate Change (IPCC). Cambridge University Press: Cambridge

Sharma D, Das GA, Babel MS (2007) Spatial disaggregation of bias-corrected GCM precipitation for improved hydrologic simulation: Ping River Basin, Thailand. Hydrol Earth Syst Sci 11:1373–1390. https://doi.org/10.5194/hessd-4-35-2007

Shi C, Jiang ZH, Chen WL, Li L (2018) Changes in temperature extremes over China under 1.5°C and 2°C global warming targets. Advances in Climate Change Research. https://doi.org/10.1016/j.accre.2017.11.003

Sun F, Roderick ML, Lim WH, Farquhar GD (2011) Hydroclimatic projections for the Murray-Darling Basin based on an ensemble derived from Intergovernmental Panel on Climate Change AR4 climate models. Water Resources Research 47:W00G02. https://doi.org/10.1029/2010WR009829

Taylor KE (2001) Summarizing multiple aspects of model performance in a single diagram. J Geophys Res 106(D7):7183–7192. https://doi.org/10.1029/2000JD900719

Tramblay Y, Ruelland D, Somot S et al (2013) High-resolution Med-CORDEX regional climate model simulations for hydrological impact studies: a first evaluation of the ALADIN-Climate model in Morocco. Hydrology & Earth System Sciences 17(10):3721–3739. https://doi.org/10.5194/hess-17-3721-2013

UNFCC, 2015. Report No. FCCC/CP/2015/L.9/Rev.1. http://unfccc.int/resource/docs/2015/cop21/eng/l09r01.pdf

Vrac M, Drobinski P, Merlo A et al (2012) Dynamical and statistical downscaling of the French Mediterranean climate: uncertainty assessment. Natural Hazards and Earth System Science 12(9):2769–2784. https://doi.org/10.5194/nhess-12-2769-2012

Wang T, Miao JP, Sun JQ, Fu YH (2018) Intensified East Asian summer monsoon and associated precipitation mode shift under the 1.5°C global warming target. Advances in Climate Change Research. https://doi.org/10.1016/j.accre.2017.12.002

Wood A, Leung LR, Sridhar V, Lettenmaier DP (2004) Hydrologic implications of dynamical and statistical approaches to downscaling climate outputs. Clim Chang 62:189–216. https://doi.org/10.1023/b:clim.0000013685.99609.9e

Yang H, Jiang ZH, Li L (2016) Biases and improvements in three dynamical downscaling climate simulations over China. Clim Dyn 47(9–10):3235–3251. https://doi.org/10.1007/s00382-016-3023-9

Yang H, Jiang ZH, Li L, Wang XF, Cui CG (2017) Applicability of a quantile-quantile (Q-Q) bias-correction method for climate dynamical downscaling at Beijing station. Acta Meteorologica Sinica 75(3):460–470

Yang Y, Tang JP, Wang SY, Liu G (2018) Differential impacts of 1.5°C and 2°C warming on extreme events over China using statistically downscaled and bias-corrected CESM low-warming experiment. Geophys Res Lett. https://doi.org/10.1029/2018GL079272

Yu ET, Sun JQ, Chen HP et al (2015) Evaluation of a high-resolution historical simulation over China: climatology and extremes. Clim Dyn 45(7):2013–2031. https://doi.org/10.1007/s00382-014-2452-6

Yu R, Zhai PM, Lu YY (2018) Implications of differential effects between 1.5 and 2◦C global warming on temperature and precipitation extremes in China's urban agglomerations. Int J Climatol 38:2374–2385. https://doi.org/10.1002/joc.5340

Zhai PM, Yu R, Zhou BQ, Chen Y, Guo JP, Lu YY (2017) Research progress in impact of 1.5°C global and regional scales. Advances in Climate Change Research 13(5):465–472. https://doi.org/10.12006/j.issn.1673-1719.2017.159

Zhang YJ, Fu L, Pan J et al (2017) Projected changes in temperature extremes in China using PRECIS. Atmosphere 8(1):15. https://doi.org/10.3390/atmos8010015

Zhou TJ, Yu RC (2006) Twentieth-century surface air temperature over China and the globe simulated by coupled climate models. J Clim 19:5843–5858. https://doi.org/10.1175/JCLI3952.1

Zhou BT, Wen HQZ, Xu Y, Song LC, Zhang XB (2014) Projected changes in temperature and precipitation extremes in China by the CMIP5 multimodel ensembles. J Clim 27:6591–6611. https://doi.org/10.1175/JCLI-D-13-00761.1

Affiliations

Lianyi Guo [1,2] · Zhihong Jiang [1] · Deliang Chen [2] · Hervé Le Treut [3] · Laurent Li [3]

[1] Key Laboratory of Meteorological Disaster, Ministry of Education, Joint International Research Laboratory of Climate and Environment Change, Collaborative Innovation Center on Forecast and Evaluation of Meteorological Disasters, Nanjing, China

[2] Regional Climate Group, Department of Earth Sciences, University of Gothenburg, Gothenburg, Sweden

[3] Laboratoire de Météorologie Dynamique, CNRS, Sorbonne Université, Ecole Normale Supérieure, Ecole Polytechnique, Paris, France